Organic & Supramolecular Chemistry

Ecofriendly and Facile One-Pot Multicomponent Synthesis of 5-Phenyl-5,10-dihydropyrido[2,3-d:6,5-d′]dipyrimidine-2,4,6,8(1*H*,3*H*,7*H*,9*H*)-tetraone Derivatives Catalyzed by Cu^{II} Immobilized on Functionalized Magnetic Mesoporous MCM-41 (Fe_3O_4@MCM-41-GPTMS-Gu-Cu^{II})

Mozhgan Mazloum Farsi Baf, Batool Akhlaghinia,* Zeinab Zarei, and Sara S. E. Ghodsinia[a]

In the present study, Cu^{II} immobilized on functionalized magnetic mesoporous MCM-41 (Fe_3O_4@MCM-41-GPTMS-Gu-Cu^{II}) was prepared as a new, versatile, and magnetically nanocatalyst and characterized by FT-IR, XRD, small-angle XRD, BET, TEM, SEM, EDX, EDX-mapping, TGA, VSM, XPS, and ICP techniques. The characterizations show the presence of MCM-41 with a hexagonal structure, superparamagnetic behavior, and an average particle size of 8–25 nm. The catalytic activity of the nanocatalyst was evaluated towards the synthesis of structurally different 5-phenyl-5,10-dihydropyrido[2,3-d:6,5-d′] dipyrimidine-2,4,6,8(1*H*,3*H*,7*H*,9*H*) tetraone derivatives through one-pot multicomponent condensation under green conditions. Fe_3O_4@MCM-41-GPTMS-Gu-Cu^{II} catalyzed many consecutive trials at least five runs. High to excellent yields in short reaction times, simple procedure, environmental friendliness, less toxic solvents, high stability, and reusability of the catalyst are considerable advantages of the prepared catalytic system.

Introduction

In 1991, the green chemistry concept (with 12 principles) was first introduced, which applies to all aspects of chemistry to reach a considerable development in chemical technology regarding an environmental and economic perspective. Nowadays, this strategy, which generally leads to higher economic growth, elimination of hazardous substances, saving energy, protection of the environment, better use of resources, and also waste management, is of great importance among researchers due to the spread of pollution in the world.[1] The construction of new substances and syntheses and the emerging technologies are among the achievements of the current strategy and its continuous advances. In this sense, the rational and efficient designing of new heterogeneous catalysts is one of the fundamental pillars of modern organic synthesis, which opens a new window to achieving greener reaction protocols and thus pursues the green chemistry goals.[2,3] Interestingly, one of the most critical objectives in designing heterogeneous catalyst systems is the creating of active sites of catalytic species through covalent immobilization of metals, Schiff base ligands, or complexes on the solid supports place. These results in the adsorption of the reactants on the surface of the solid support where catalysis reaction takes place, and as a result, it enhances the concentration of the reactants on the surface and results in higher yield.[3] In this regard, so far different solid supports such as silica, carbon, zirconia, clay, zeolite, metal oxide polymers, carbon nanotubes, graphene, and other mesoporous materials have been applied in chemical synthesis and sustainable transformations.[4] Among various solid supports, ordered mesoporous silica MCM-41 with a regular pore diameter, as a highly versatile solid support, has demonstrated fascinating properties. This includes a featuring hexagonal arrangement of one-dimensional pores, high thermal stability, modifiable surfaces, biocompatibility, excellent physicochemical stability, very narrow pore size distribution, chemical, and mechanical stability, stunning surface area (700–1100 $m^2 g^{-1}$), controllable morphologies, and large pore size. Thereby, mesoporous silica MCM-41 has particularly a great potential that can be used as a heterogeneous catalyst or versatile solid support.[5] This allows the entrapment of organic reactants and their passage to reach the surface of the channels. Besides, the surface of this class of silicate compounds can be easily modified with organosilane agents through a significant number of silanol groups on the surface of its channels, which results in the increased absorption capacity.[6] Although MCM-41 is a right candidate thanks to its aforementioned extraordinary properties, it often involves long, and tedious procedures and strategies for filtration such as centrifugation, due to the nanosize of the catalyst particles that prevents their utilization in liquid-solid processes. Therefore, incorporation of magnetic nanoparticles (Fe_3O_4 NPs) can enable quick, easy and efficient separation of the catalyst from the reaction mixture under an external magnetic field owing to its

[a] *M. M. F. Baf, Dr. B. Akhlaghinia, Dr. Z. Zarei, Dr. S. S. E. Ghodsinia*
Department of Chemistry Faculty of Science, Ferdowsi University of Mashhad, Mashhad 9177948974, Iran
E-mail: akhlaghinia@um.ac.ir

Supporting information for this article is available on the WWW under https://doi.org/10.1002/slct.202004112

paramagnetic nature, and then help to resolve this problem and promote the catalytic performance.[5]

Today, from green chemistry perspectives, multicomponent reactions (MCRs) (as a recognized powerful tool in modern synthetic organic chemistry) happening in one step using a heterogeneous catalyst is incorporated to provide quick access and afford expected new organic molecules or automated high conversion of reactants into products with higher productivity. This leads to a decrease in the consumption of reagents and solvents and causes minimization of waste, energy, and time and results in a less hazardous solvent, cleaner auxiliaries, good atom-economy, higher selectivity compared with multi-step reactions which satisfy main principles of green chemistry.[7–10]

1,4-Dihydropyridines (as nitrogen-containing heterocycles) with a structure analogous to nicotinamide adenine dinucleotide (NAD) coenzyme have attracted considerable interest due to their different biological and medicinal applications.[7,11–21] They have increasingly-popular worldwide applications such as antitumor, antisclerotic, antidiabetic, calcium channel blockers, anti-inflammatory, and analgesic.[22] Literature studies clearly show that they also have anti-TB activity owing to their lipophilic groups and can be used in tumor and Alzheimer's disease therapy as well.[23,24] In the meantime, an essential group of heterocyclic frameworks containing 1,4-dihydropyridines core is 5-phenyl-5,10-dihydropyrido[2,3-d:6,5-d′]dipyrimidine-2,4,6,8(1*H*,3*H*,7*H*,9*H*)-tetraone derivatives which have attracted considerable attention due to their broad spectrum of promising biological activities and medicinal applications.[25] Numerous reports represent anticorrosive,[26] antimicrobial,[27] antitubercular,[28] antiviral, and cytotoxic activities[29] of these compounds (Scheme 1). Moreover, a few numbers of such derivatives have significant α-glucosidase and α-amylase inhibitory activity.[30] These heterocyclic compounds can self-assemble to constitute a supramolecular structure as well.[31] Therefore, many different strategies have been developed to synthesize various structures of 5-phenyl-5,10-dihydropyrido [2,3-d:6,5-d′]dipyrimidine-2,4,6,8(1*H*,3*H*,7*H*,9*H*)-tetraone derivatives such as using DIPEA, $[H\text{-}NMP]^+[HSO_4]^-$,γ-$Fe_2O_3$@HAp-$SO_3H$, nano-[DMSPDE][Cl], Fe-MCM-41-ionic liquid, nano-$CuFe_2O_4$, and $CuFe_2O_4$ nanospheres.[32–34] These techniques suffer particular drawbacks such as unwanted by-products, using organic solvents, base, heating and/or refluxing condition, and ultrasound irradiation or tedious procedure of catalyst preparation, which are not in agreement with the green chemistry strategies. Consequently, in order to overcome these kinds of problems, a continued pursuit for reaching greener, simpler, more convenient, and environmentally-friendly approaches are still paramount.

Encouraged by the prominence of 5-phenyl-5,10-dihydropyrido[2,3-d:6,5-d′]dipyrimidine-2,4,6,8(1*H*,3*H*,7*H*,9*H*)-tetraone derivatives, and in continuation to our endeavors in the synthesis of various heterocyclic molecules using new heterogeneous catalyst systems[35] and the versatility of $Cu(OAc)_2 \cdot H_2O$, herein for the first time, we introduced Cu^{II} immobilized on functionalized magnetic mesoporous MCM-41 (Fe_3O_4@MCM-41-GPTMS-Gu-Cu^{II}) as a novel and separable heterogeneous nanocatalyst. In this approach, guanidinium salt was grafted on the surface of functionalized magnetic MCM-41 and then followed by immobilization of $Cu(OAc)_2$, as seen in Scheme 2. It is worth to note that $Cu(OAc)_2$ as Lewis acid along with grafted guanidinium (as a bidentate, cationic hydrogen-bond donor ligand and weak Brønsted acid acts as a metal-free "*p*-Lewis acid" site[36,37]) can activate carbonyl groups of reactants and cause faster attacking of ammonium acetate (see the suggested mechanism in Scheme 4).

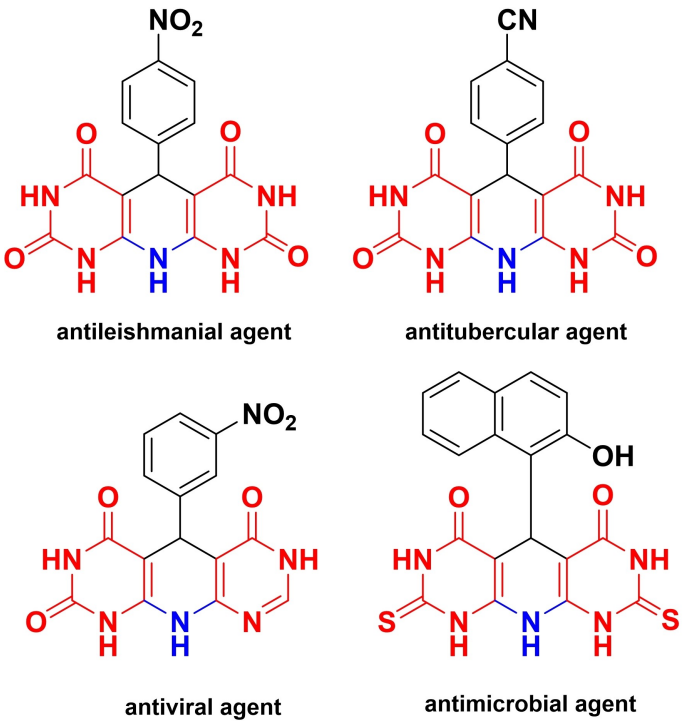

Scheme 1. Structure of some components as drug molecules.

Then, the catalytic activity of the synthesized nanocatalyst was examined to access 5-phenyl-5,10-dihydropyrido[2,3-d:6,5-d′]dipyrimidine-2,4,6,8(1*H*,3*H*,7*H*,9*H*)-tetraone derivatives *via* the one-pot multicomponent reactions between different aldehydes, barbituric acid, and ammonium acetate (as a nitrogen source) in water as the best solvent which is following sustainable chemistry (Scheme 3). Green condition, short reaction time, no need for column chromatographic purification, high yields of desired products, and cutting down the handling costs due to simple working procedures are among the privileged features of this proposed catalytic system. Therefore, it seems that this nanocatalyst could be utilized for other reactions, which need Lewis acid sites.

Results and Discussion

Characterization of Cu^{II} immobilized on functionalized magnetic mesoporous MCM-41 (Fe_3O_4@MCM-41-GPTMS-Gu-Cu^{II})

In the present study, Fe_3O_4@MCM-41-GPTMS-Gu-Cu^{II} (**V**) as a heterogeneous nanostructured catalyst was prepared accord-

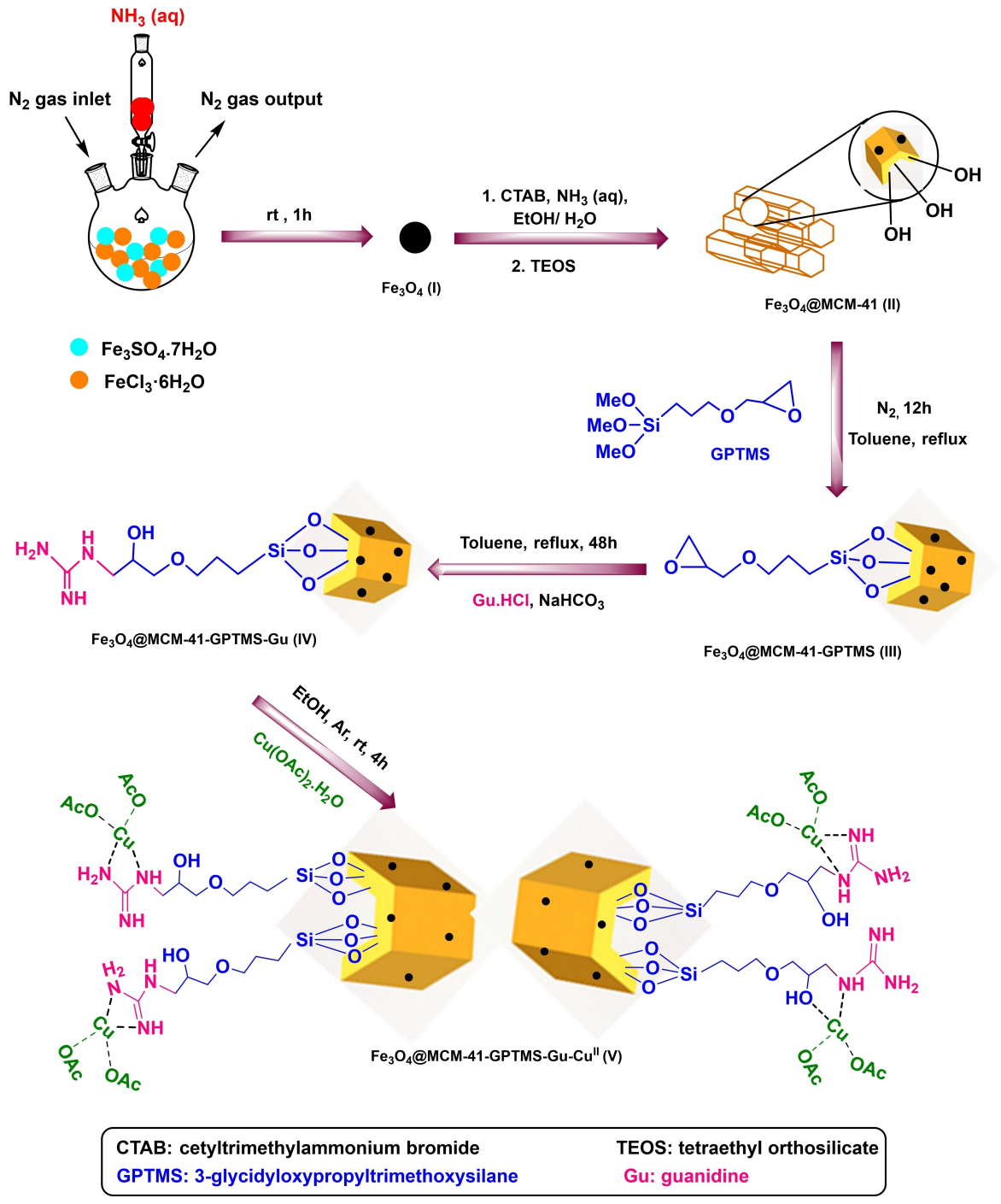

Scheme 2. Preparation of Cu^{II} immobilized on aminated 3-glycidyloxypropyl trimethoxysilane anchored on magnetic mesoporous MCM-41 (Fe_3O_4@ MCM-41-GPTMS-Gu-Cu^{II}).

ing to the five steps indicated in Scheme 1. Initially, Fe_3O_4 NPs (**I**) were prepared *via* the co-precipitation approach[35g] followed by coating with MCM-41 comprising the reaction of TEOS and CTAB to achieve Fe_3O_4@MCM-41 (**II**) after calcination at 550 °C for 6 h. After that, the hydroxyl groups on the surface of the as-synthesized Fe_3O_4@MCM-41 (**II**) were functionalized appropriately by the treatment of magnetic nanoparticles entrapped in mesoporous MCM-41 (Fe_3O_4@MCM-41 (**II**)) with 3-glycidyloxypropyltrimethoxysilane (GPTMS) and guanidine hydrochloride, respectively which yielded 3-glycidyloxypropyl trimethoxysilane anchored on magnetic nanoparticles entrapped in mesoporous MCM-41 (Fe_3O_4@MCM-41-GPTMS (**III**)) and aminated 3-glycidyloxypropyl trimethoxysilane anchored on magnetic nanoparticles entrapped in mesoporous MCM-41 (Fe_3O_4@MCM-41-GPTMS-Gu (**IV**)). Subsequently, Cu^{II} immobilized on functionalized mesoporous MCM-41 (Fe_3O_4@MCM-41-

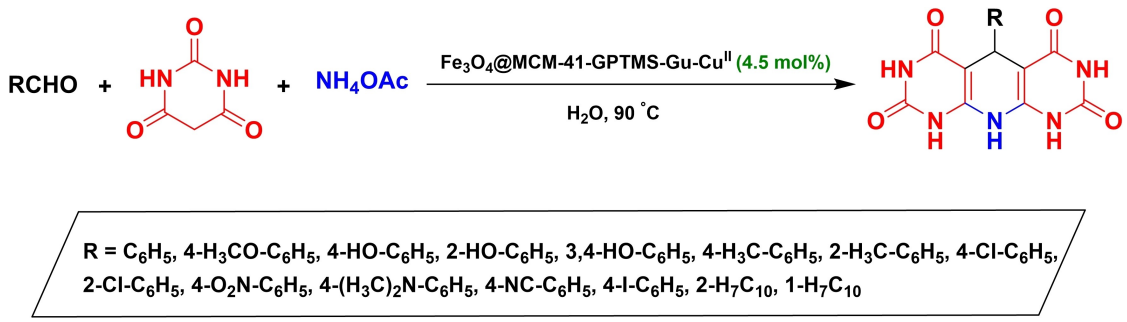

Scheme 3. Synthesis of 5-phenyl-5,10-dihydropyrido[2,3-d:6,5-d']dipyrimidine-2,4,6,8(1*H*,3*H*, 7*H*,9*H*)-tetraone derivatives in the presence of Fe_3O_4@ MCM-41-GPTMS-Gu-Cu^{II}.

GPTMS-Gu-Cu^{II} (**V**)) (with 0.9 mmol g^{-1} copper content according to the inductively coupled plasma optical emission spectroscopy (ICP-OES) measurement) with further Lewis acidic sites was obtained upon treatment of Fe_3O_4@MCM-41-GPTMS-Gu (**IV**) with an ethanolic solution of $Cu(OAc)_2.H_2O$. Then, the structural and chemical characterizations of the attained Fe_3O_4@MCM-41-GPTMS-Gu-Cu^{II} (**V**) was fully characterized by FT-IR, XRD, small-angle XRD, BET, SEM, EDX, EDX-mapping, TEM, TGA, VSM, XPS, and ICP techniques.

The chemical structure of Fe_3O_4 NPs (**I**), Fe_3O_4@MCM-41 (**II**), Fe_3O_4@MCM-41-GPTMS (**III**), Fe_3O_4@MCM-41-GPTMS-Gu (**IV**), and Fe_3O_4@MCM-41-GPTMS–Gu-Cu^{II} (**V**), was studied by FT-IR spectroscopy as illustrated in Figure 1a–e. The relatively broad vibration band appeared around 3420–3400 cm^{-1} was attributed to the asymmetric and symmetric stretching vibration modes of the hydroxyl groups on the surface of Fe_3O_4. As shown, a characteristic band at 579 cm^{-1} was also seen for the stretching vibration bands of Fe–O bonds (Figure 1a).[38] The FT-IR spectrum of Fe_3O_4@MCM-41 (**II**) (Figure 1b) showed two new absorption bands at 1088 and 800 cm^{-1} that disclosed the presence of MCM-41,[39] in addition to the bands mentioned in the Fe_3O_4 structure. In the FT-IR spectrum of Fe_3O_4@MCM-41-GPTMS (**III**) (Figure 1c), two new absorption bands, which appeared at 2942 and 2851 cm^{-1} were attributed to the stretching vibration modes of CH_2 groups.[35b] Also, anchoring of guanidine to the Fe_3O_4@MCM-41-GPTMS (**III**) surface was proven by the appearance of amazing new bands at 1669 and 1570 cm^{-1} (attributed to the ν C=N of guanidine groups and the ν NH of $-NH_2$ groups) (Figure 1d).[40] Interestingly, the decreasing intensities of absorption bands at 1665 and 1575 cm^{-1} suggested the successful coordination of Cu $(OAc)_2 \cdot H_2O$ (Figure 1e).

Furthermore, XRD analysis was implemented to perceivethe purity, phase, and crystallinity of the synthesized Fe_3O_4@MCM-41 (**II**) and Fe_3O_4@MCM-41-GPTMS-Gu-Cu^{II} (**V**) nanocatalyst (Figure 2). As is seen from the diffractogram of Fe_3O_4@MCM-41 (**II**), the presence of five characteristic peaks at $2\theta = 62.4°$, 57.0°, 53.5°, 35.4°and 30.2°, which were attributed to (4 4 0), (5 1 1), (4 4 2), (3 1 1), and (2 2 0) reflection planes, respectively, were

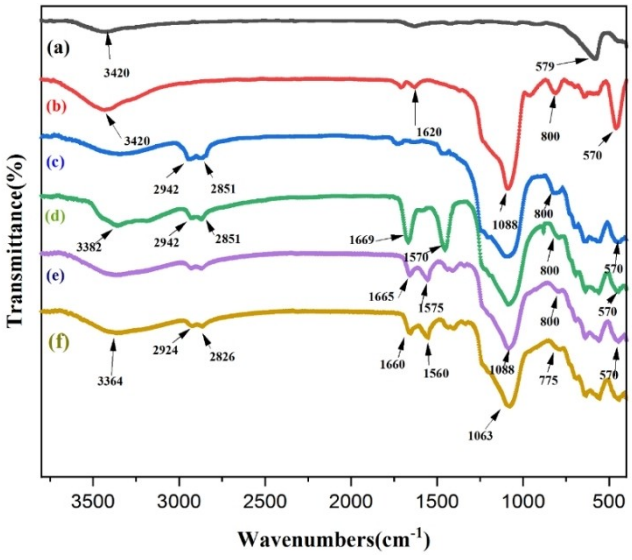

Figure 1. FT-IR spectra of (a) Fe_3O_4 (**I**), (b) Fe_3O_4@MCM-41 (**II**), (c) Fe_3O_4@MCM-41-GPTMS (**III**), (d) Fe_3O_4@MCM-41-GPTMS-Gu (**IV**), (e) Fe_3O_4@MCM-41-GPTMS-Gu-Cu^{II} (**V**) and (f) 5th reused Fe_3O_4@MCM-41-GPTMS-Gu-Cu^{II} (**V**).

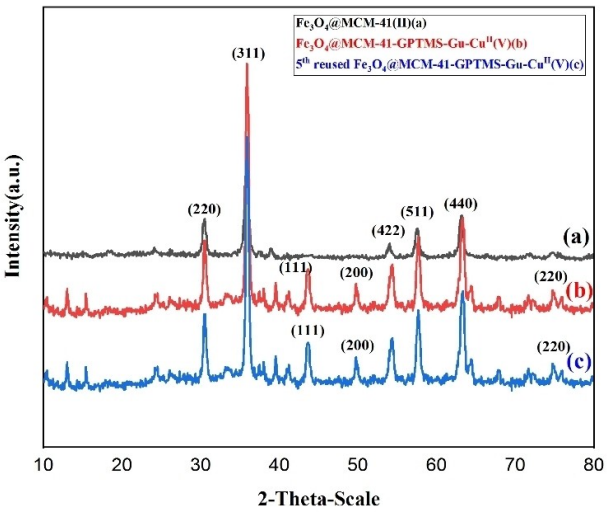

Figure 2. The XRD patterns of (a) Fe_3O_4@MCM-41 (**II**), (b) Fe_3O_4@ MCM-41-GPTMS-Gu-Cu^{II} (**V**) and (c) 5th reused Fe_3O_4@ MCM-41-GPTMS-Gu-Cu^{II} (**V**).

closely matched with the standard pattern for crystalline magnetite with spinel structure.[35a&b,41]

After immobilization of Cu^{II}, three new diffraction peaks were observed at $2\theta = 74.3°$, 50.6° and 43.4° corresponding to (2 2 0), (2 0 0) and (1 1 1) planes, respectively. This can be an account of the existence of Cu element (JCPDS: 4-0836)[42] in the nanocatalyst structure. The crystallite size of Fe_3O_4@MCM-41-GPTMS-Gu-Cu^{II} (**V**) nanocatalyst was estimated to be 21 nm, according to the Deby-Scherer equation.

The small-angle powder X-ray diffraction pattern of Fe_3O_4@MCM-41 (**II**) showed a broad peak at $2\Theta = 2.75$, attributing to (1 0 0) reflection plane with high intensity, which could be owing to the presence of MCM-41 support (possessing a well-defined two-dimensional hexagonal structure with a high degree of long-range order and existence of uniform pores[43]) (Figure 3a).

This was also preserved in the pattern of Fe_3O_4@MCM-41-GPTMS-Gu-Cu^{II} (**V**) nanocatalyst (Figure 3b), representing the high stability of the structure of the designed nanocatalyst. Notably, compared to the pattern of Fe_3O_4@MCM-41 (**II**), a decreasing intensity peak confirmed functionalization of MCM-41 channels during preparation steps of Fe_3O_4@MCM-41-GPTMS-Gu-Cu^{II} (**V**).[44]

The nitrogen adsorption-desorption isotherms and pore size distribution curves of Fe_3O_4@MCM-41 (**II**) and Fe_3O_4@MCM-41-GPTMS-Gu-Cu^{II} (**V**) are presented in Figure 4a–c. As demonstrated in Figure 4a, Fe_3O_4@MCM-41 (**II**) and Fe_3O_4@MCM-41-GPTMS-Gu-Cu^{II} (**V**) exhibited the characteristics of type IV isotherms as reported by the IUPAC classification of adsorption isotherms with

H1-type hysteresis loop[45a] (which is a characteristic of ordered mesoporous materials) (Figure 4 a). The specific surface area, pore-volume, and mean pore diameter of Fe_3O_4@MCM-41 (**II**) and Fe_3O_4@MCM-41-GPTMS-Gu-Cu^{II} (**V**) are shown in Table 1. It is observed that both the surface area and total

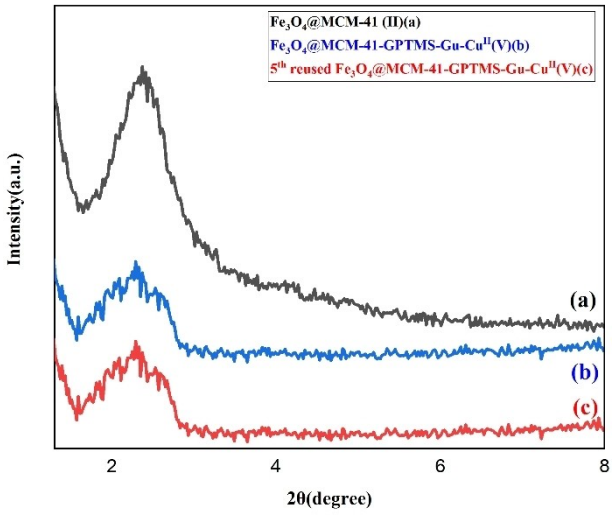

Figure 3. Small-angle XRD patterns of (a) Fe_3O_4@MCM-41 (**II**), (b) Fe_3O_4@MCM-41-GPTMS-Gu-Cu^{II} (**V**) and (c) 5th reused Fe_3O_4@MCM-41-GPTMS-Gu-Cu^{II} (**V**).

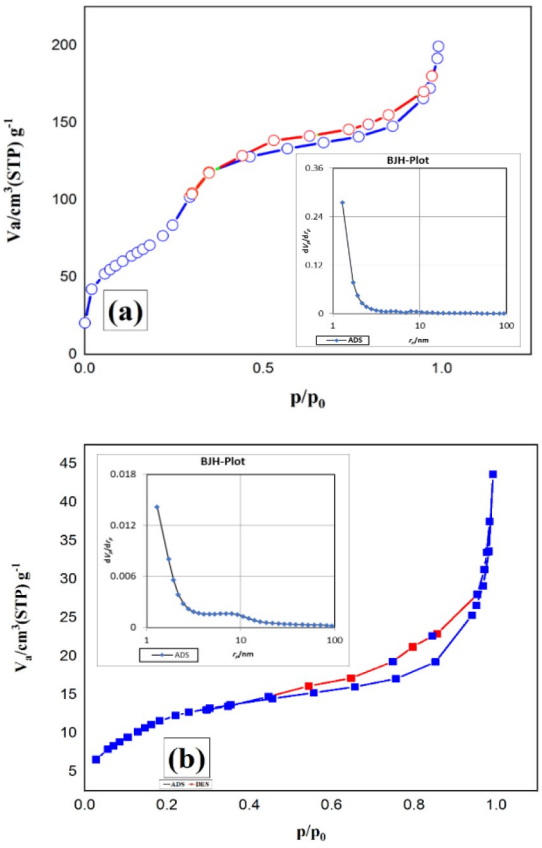

Figure 4. Nitrogen adsorption-desorption isotherms and pore size distribution curves of (a) Fe_3O_4@MCM-41 (**II**) and (b) Fe_3O_4@MCM-41-GPTMS-Gu-Cu^{II} (**V**).

Table 1. Total pore volume, specific surface area, and mean pore diameter of Fe_3O_4@MCM-41 (**II**) and Fe_3O_4@ MCM-41-GPTMS-Gu-Cu^{II} (**V**).

Sample	Total pore volume ($cm^3 g^{-1}$)	S_{BET} ($m^2 g^{-1}$)	Mean pore diameter (nm)
Fe_3O_4@MCM-41 (**II**)	0.305	262.82	4.642
Fe_3O_4@MCM-41-GPTMS-Gu-Cu^{II} (**V**)	0.0642	44.88	5.723

porevolume decreased in Fe_3O_4@MCM-41-GPTMS-Gu-Cu^{II} (**V**) nanocatalyst, compared to Fe_3O_4@MCM-41 (**II**), which may be explained as a result of the occupation of some pores by anchored organic segments, which took place during the functionalization process and also immobilization of Cu^{II}.[45b&c] It is noteworthy that increasing mean pore, compared to Fe_3O_4@MCM-41 (**II**), is probably corresponding to the presence of Cu^{II}, which causes the creation of new pores in the structure of Fe_3O_4@MCM-41-GPTMS-Gu-Cu^{II} (**V**).[46]

The morphology of Fe_3O_4@MCM-41 (**II**) and Fe_3O_4@MCM-41-GPTMS-Gu-Cu^{II}(**V**) nanocatalyst was also explored by scanning electron microscopy (SEM) technique (Figure 5). As clearly shown in Figure 5a, Fe_3O_4@MCM-41 (**II**) and Fe_3O_4@MCM-41-

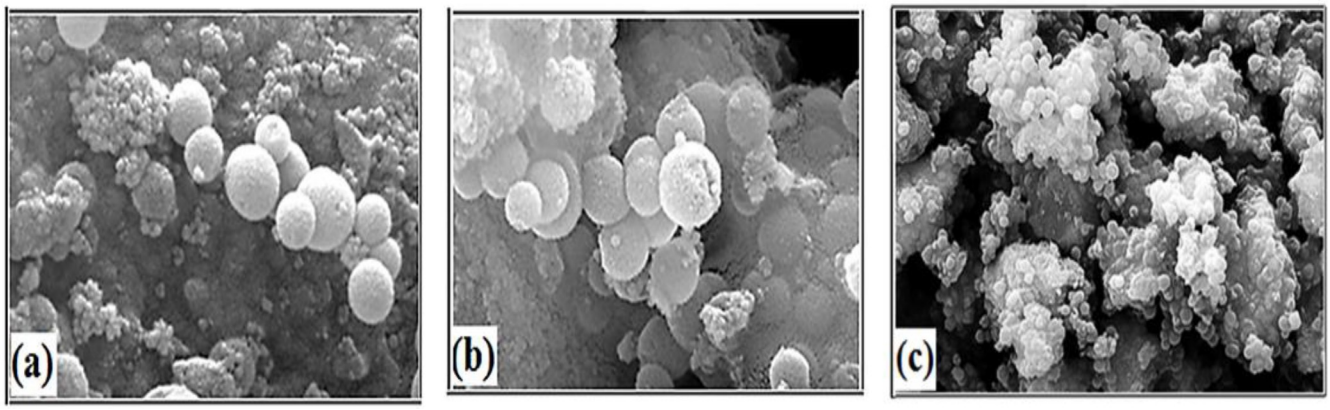

Figure 5. SEM image of (a) Fe_3O_4@MCM-41 (**II**), (b) Fe_3O_4@MCM-41-GPTMS-Gu-Cu^{II} (**V**) and (c) 5th reused Fe_3O_4@ MCM-41-GPTMS-Gu-Cu^{II} (**V**).

GPTMS-Gu-Cu^{II} (**V**) have an almost irregular spherical morphology.

These results demonstrate that there was no significant change in surface morphology of Fe_3O_4@MCM-41 (**II**) after functionalization processes, verifying chemical stability.

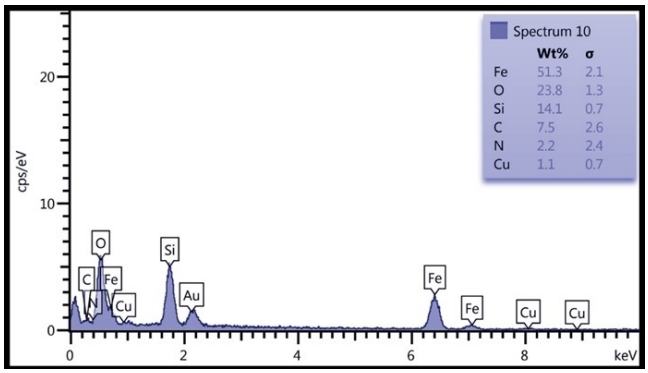

Figure 6. EDX spectrum of Fe_3O_4@MCM-41-GPTMS-Gu-Cu^{II} (**V**).

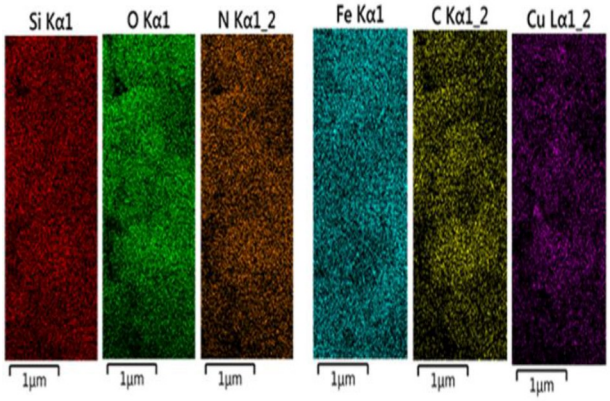

Figure 7. EDX-mapping analysis of Fe_3O_4@ MCM-41-GPTMS-Gu-Cu^{II} (**V**).

Additionally, the formation of Fe_3O_4@MCM-41-GPTMS-Gu-Cu^{II} (**V**) can be authorized by EDX analysis. As illustrated in Figure 6, the presence of signals of Si, N, O, and Cu elements in the nanocatalyst structure, was evidence of successful surface functionalization of Fe_3O_4@MCM-41 (**II**), and then immobilization of Cu^{II} on it.

To further the evaluate elemental composition on the surface of nanocatalyst, and EDX-mapping analysis was used and the results are shown in Figure 7. As can be seen, all elements of the functional groups (Si, O, N, Fe, C, and Cu) that were anchored on the surface of the nanocatalyst structure are homogeneously distributed.The morphology of Fe_3O_4@MCM-41 (**II**) and Fe_3O_4@MCM-41-GPTMS-Gu-Cu^{II} (**V**) nanocatalyst was further examined using transmission electron microscopy (TEM) analysis, as is depicted in Figure 8. Notably, TEM images of the core-shell Fe_3O_4@MCM-41 and Fe_3O_4@MCM-41-GPTMS-Gu-Cu^{II} are shown in Figure 8a—d. It was clearly observed in Figure 8a & b, that the Fe_3O_4 NPs core is well encapsulated by mesoporous silica MCM-41 coating with a clear boundary between the mesoporous silica shell and the Fe_3O_4 NPs core. The dispersed state of these magnetic particles in mesoporous MCM-41 determines the shape and size of the catalyst particles,[8] which agrees well with the TEM observation (Figure 8c & d). As can be seen in Figure 8c & d, the finally formed sample (**V**) demonstrated the formation of a core-shell structure with an average size of 8 to 25 nm (according to particle size distributions inset in Figure 9).

Thermal stability of Fe_3O_4@MCM-41 (**II**), Fe_3O_4@MCM-41-GPTMS (**III**), Fe_3O_4@MCM-41-GPTMS-Gu (**IV**), and Fe_3O_4@MCM-41-GPTMS-Gu-Cu^{II} (**V**) was also studied using TGA analysis at a temperature between 25–900 °C (Figure 10 a–d). As can be illustrated in Figure 10a, Fe_3O_4@MCM-41 (**II**) has one weight loss step (9%), which is due to physisorbed water molecules on the surface of it.[47] However, Fe_3O_4@MCM-41-GPTMS (**III**) showed two mass loss steps; 25–150 °C (2.9%), which was ascribed to the physically-adsorbed water, and above 150 °C which was due to thermal decomposition of organic segments of Fe_3O_4@MCM-41-GPTMS (**III**) (21.3%) (Figure 10 b). Interestingly, Fe_3O_4@MCM-41-GPTMS-Gu (**IV**) has three weight loss

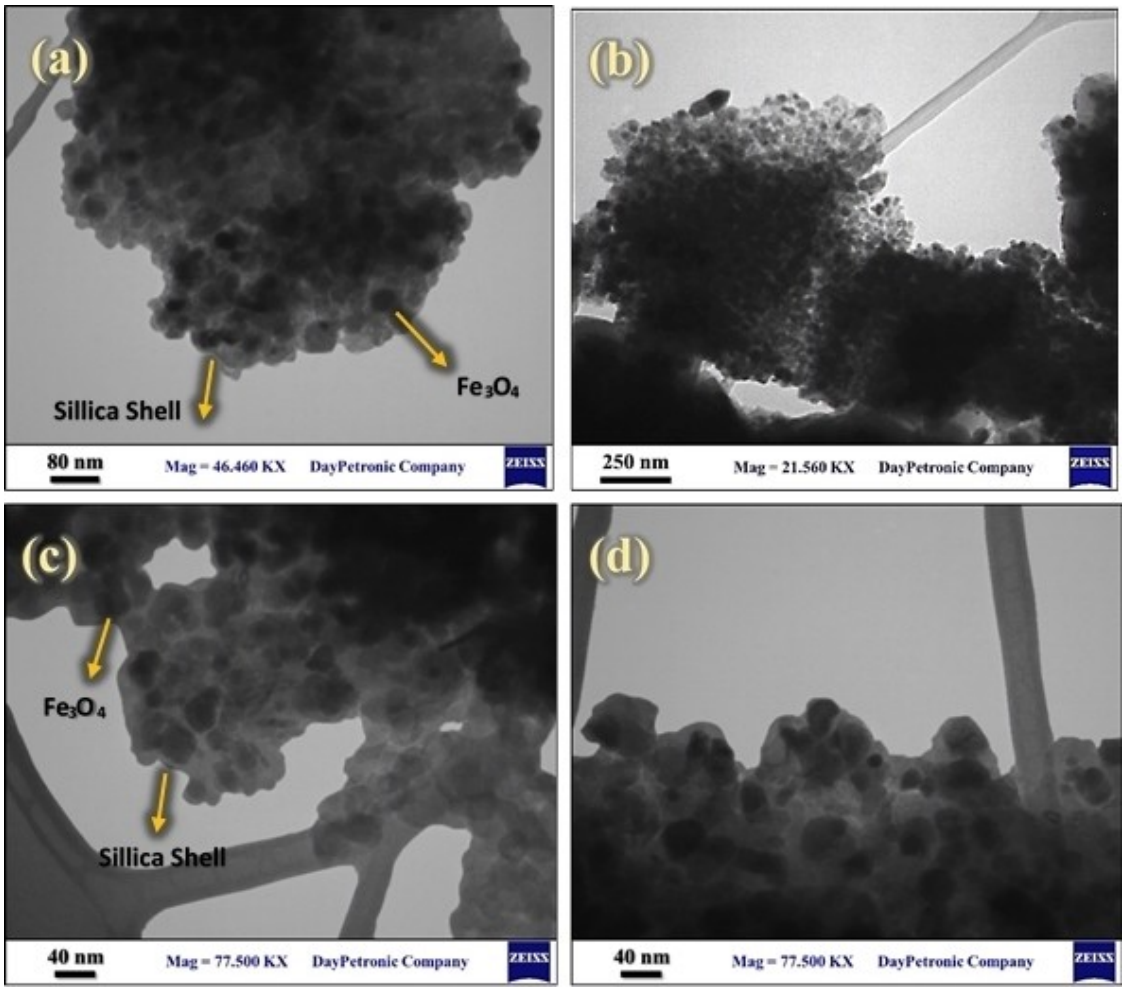

Figure 8. TEM images of (a and b) Fe_3O_4@MCM-41 (**II**) and (c and d) Fe_3O_4@ MCM-41-GPTMS-Gu-Cu^{II} (**V**).

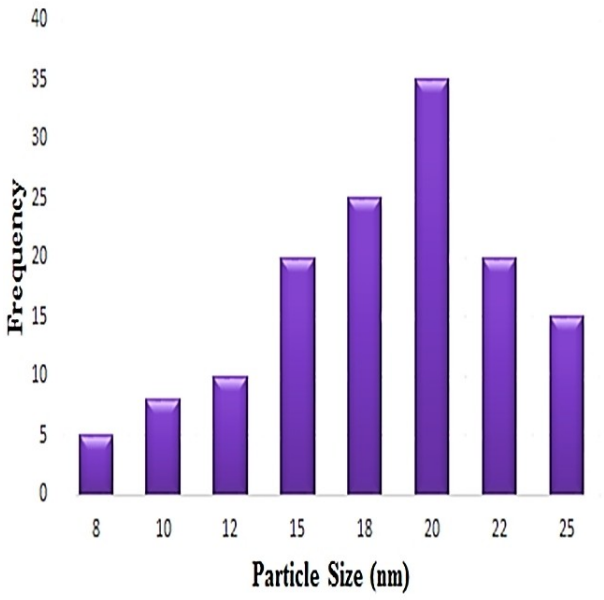

Figure 9. Particle size distribution histogram of Fe_3O_4@ MCM-41-GPTMS-Gu-Cu^{II} (**V**).

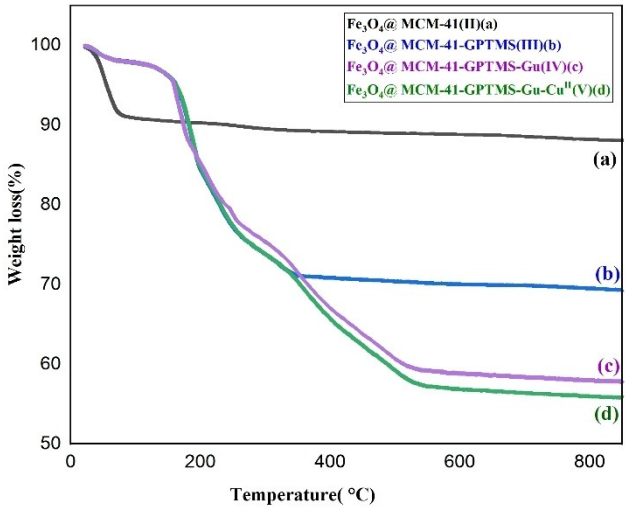

Figure 10. TGA thermograms of (a) Fe_3O_4@MCM-41 (**II**), (b) Fe_3O_4@MCM-41-GPTMS (**III**), (c) Fe_3O_4@ MCM-41-GPTMS-Gu (**IV**), and (d) Fe_3O_4@ MCM-41-GPTMS-Gu-Cu^{II} (**V**).

steps in which the first mass loss started from 25–150 °C (corresponded to the removal of water), and the second step related to the decomposition of organic molecules started from 150–350 °C (15.4%). Above this temperature (>350 °C), the structure of Fe_3O_4@MCM-41-GPTMS-Gu (**IV**) was entirely disintegrated (10%) (Figure 10 c). Similarly, the thermal decomposition curve of Fe_3O_4@MCM-41-GPTMS-Gu-Cu^{II} (**V**) indicated three significant mass changes. The weight loss before 150 °C, resulted from the loss of the trapped physically-adsorbed water. The next step happened at 150–250 °C (13%), which can be attributed to the elimination of organic segments anchored on Fe_3O_4@MCM-41(**II**). Finally, the last step, which was at around 250 °C and continued up to 560 °C (12%), was due to the complete decomposition of the nanocatalyst and silanol groups (Figure 10d).[44,47] Based on the TGA results, the amounts of organic linkers anchored on Fe_3O_4@MCM-41(**II**) was evaluated to be 1 mmol g^{-1}. These findings are in perfect accordance with the results obtained from elemental analysis data (N = 1.71% and C = 4.16%). Additionally, ICP analysis represented that the total immobilized copper content in the freshly prepared catalyst was 57.150 ppm/or 0.057 g/or 0.900 mmol of Cu per 1 g of catalyst.

In the next phase, the magnetic features of Fe_3O_4 (**I**) and Fe_3O_4@MCM-41-GPTMS-Gu-Cu^{II}(**V**) were determined by vibrating sample magnetometer (VSM) analysis at room temperature, as can be seen in Figure 11. According to this analysis, the saturation magnetization of Fe_3O_4@MCM-41-GPTMS-Gu-Cu^{II} (**V**) was measured to be 60 emu/g, which declined compared with those of Fe_3O_4 (**I**) (70 emu/g) (Figure 11 a). It is clear that based on literature,[35a] this decrease is due to the successful modification of the surface of Fe_3O_4@MCM-41 (**II**). It is worth noting that the easy separation of the desired nanocatalyst by placing an external magnet experimentally represents that the nanocatalyst has superparamagnetic behavior, as can be seen from the magnetization curve (Figure 11 b).

To achieve a better insight into the oxidation state of the Cu ions immobilized on functionalized magnetic mesoporous MCM-41, X-ray photoelectron spectroscopy (XPS) analysis was carried out for both fresh NPs (**IV**) and the 5th recovered nanocatalyst (Figure 12a & b). The Cu2p spectrum of fresh nanocatalyst indicates that Cu is present only as Cu^{+2} ions by two spin-orbit doublets with strong satellite peaks. As observed in Figure 12a, binding energy peaks at 933.6 eV and 953.4 eV can be attributed to Cu2p3/2 and Cu2p1/2 spin-orbit split-doublets, respectively, which are characteristic of Cu in +2 oxidation state.[48]

Catalytic synthesis of 5-phenyl-5,10-dihydropyrido [2,3-d:6,5-d′]dipyrimidine-2,4,6,8(1*H*,3*H*,7*H*,9*H*)-tetraone derivatives

Due to our continuing substantial interest in green chemistry (by applying heterogeneous catalysts in various organic transformations),[35] after successful preparation and full struc-

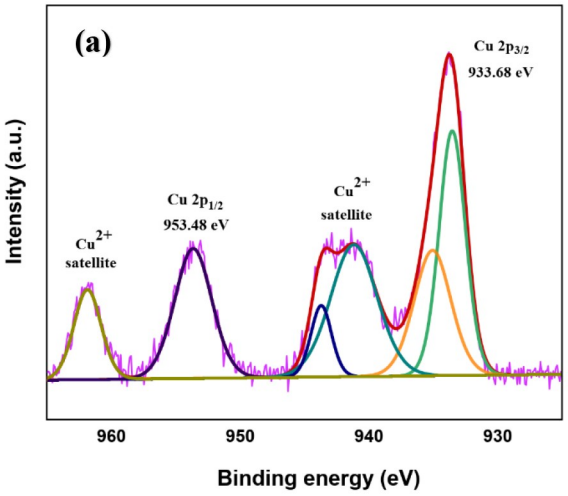

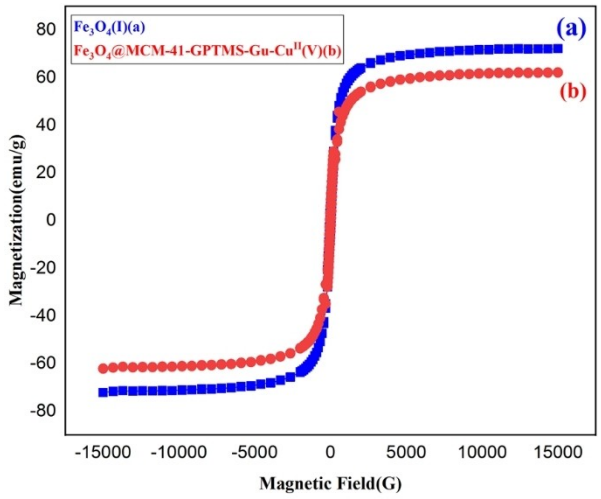

Figure 11. Magnetization curves of (a) Fe_3O_4 (**I**) and (b) Fe_3O_4@ MCM-41-GPTMS-Gu-Cu^{II} (**V**).

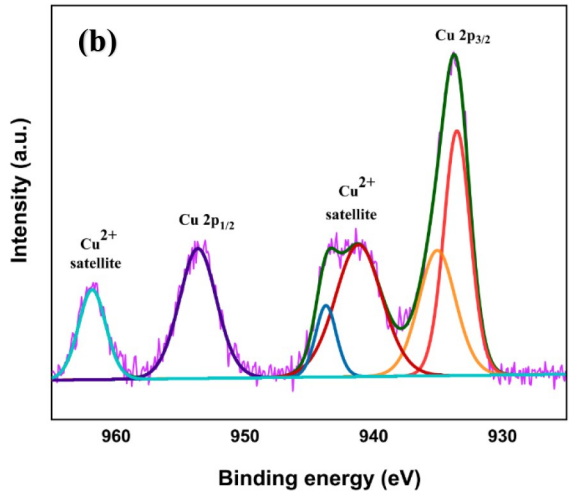

Figure 12. XPS spectra of (a) fresh Fe_3O_4@ MCM-41-GPTMS-Gu-Cu^{II} (**V**) and (b) 5th reused Fe_3O_4@ MCM-41-GPTMS-Gu-Cu^{II} (**V**).

tural characterization of Fe_3O_4@MCM-41-GPTMS-Gu-Cu^{II}, the catalytic activity of this magnetic nanostructured catalyst was explored in the preparation reaction of dihydropyrido[2,3-d:6,5- d′]dipyrimidine derivatives (Scheme 2).In our initial study, an optimum reaction profile for preparation of 5-phenyl-5,10-dihydropyrido[2,3-d:6,5-d′]dipyrimidine-2,4,6,8(1*H*,3*H*,7*H*,9*H*)-tetraone was investigated *via* one-pot multicomponent reaction of benzaldehyde(0.5 mmol), barbituric acid (1 mmol), and ammonium acetate (0.8 mmol) as a model reaction by taking into consideration various important parameters including the catalyst loading, solvent, and temperature in the presence of Fe_3O_4@MCM-41-GPTMS-Gu-Cu^{II}. The screening of various conditions is presented in Table 2. At the outset, to elucidate the catalyst's role, it was observed that in a refluxing mixture of water/ ethanol (5:1) and the absence of catalyst, the model reaction led to a 50% yield of the desired product after a long time. (Table 2, entry 1). During our optimization studies, Table 2 shows that by applying the same reaction conditions, the model reaction was progressed smoothly in the presence of Fe_3O_4@MCM-41-GPTMS-Gu-Cu^{II} (Table 2, entry 2). In a set of experiments, the model reaction was conducted in the presence of different amounts of the catalyst loading (Table 2, entries 2–7). Pleasantly, it was found that the maximum yield of the desired product was obtained in 30 min by applying a 4.5 mol% catalysts. To search for the best solvent system, the model reaction was performed by applying 4.5 mol% of Fe_3O_4@MCM-41-GPTMS-Gu-Cu^{II} in H_2O owing to environmental awareness, cost-effectiveness, and easy accessibility of H_2O. It was found that the reasonable yield of the desired product (97% after 30 min) was achieved when the model reaction was performed in refluxing H_2O (Table 2, entry 8). Then, the model reaction's feasibility was examined at room temperature, 80 °C, and 90 °C (Table 2, entries 9–11). Interestingly, the obtained results revealed that the best catalytic activity of Fe_3O_4@MCM-41-GPTMS-Gu-Cu^{II} was gained in H_2O at 90 °C (97%, 30 min (Table 2, entry 11). In further attempts, to emphasize the essential role of Fe_3O_4@MCM-41-GPTMS-Gu-Cu^{II} and also to study the effect of grafted guanidine and immobilized $Cu(OAc)_2.H_2O$, in the preparation of dihydropyrido[2,3-d:6,5- d′]dipyrimidine derivatives, several sets of reactions were performed in presence of Fe_3O_4 NPs (**I**), Fe_3O_4@MCM-41 (**II**) and Fe_3O_4@ MCM-41-GPTMS (**III**) as catalyst (Table 2, entries 12–15). Comparatively, the low yield of the desired product was obtained after prolonged reaction time in all cases (due to Lewis acidity of Fe_3O_4 NPs, and influence of grafted guanidine on functionalized Fe_3O_4@MCM-41). Similarly, the model reaction in the presence of $Cu(OAc)_2.H_2O$ afforded the desired product in 55% yield after 2.5 h (Table 2, entry 16).

Encouraged by these identified optimized conditions (Table 2, entry 11), we focused our attention on generalizing the present method for the synthesis of 5-phenyl-5,10-dihydropyrido[2,3-d:6,5-d′]dipyrimidine-2,4,6,8(1*H*,3*H*,7*H*,9*H*)-tetraone derivatives through the one-pot multicomponent reactions of various aldehydes, barbituric acid, and ammonium acetate under the optimized reaction conditions. The results of this detailed study are presented in Table 3. As illustrated by the summarized data in Table 3, the reactions proceeded rapidly, and the desired 5-phenyl-5,10-dihydropyrido[2,3-d:6,5-d′]dipyrimidine-2,4,6,8(1*H*,3*H*,7*H*,9*H*)-tetraone derivatives were obtained from a diverse set of aromatic aldehydes in high yields (Table 3, entries 1–13). Comparatively, electron-poor aldehydes resulted in higher yields after a short time than electron-rich ones (Table 3 entries 2–4 *vs.* Entries 7–13). The difference in reactivity between 4-chloro benzaldehyde/or 4-hydroxy benzaldehyde and 2-chloro benzaldehyde/or 2-hydroxy benzaldehyde can be rationalized by the steric effects of Cl/or OH in the *ortho* position of the aromatic ring (Table 3, entry 4/ or 7 *vs.* entry 5/or 8). The present catalytic system was

Table 2. Optimization of various reaction parameters for the synthesis of 5-phenyl-5,10-dihydropyrido[2,3-d:6,5-d′]dipyrimidine-2,4,6,8(1*H*,3*H*,7*H*,9*H*)-tetraone.

Entry	Catalyst (mol %)	Solvent	Temp. (°C)	Time (h)	Isolated Yield (%)
1	–	H_2O/EtOH (5:1 v/v)	Reflux	22	50
2	2.4	H_2O/EtOH (5:1 v/v)	Reflux	2.5	68
3	3.4	H_2O/EtOH (5:1 v/v)	Reflux	2	80
4	3.9	H_2O/EtOH (5:1 v/v)	Reflux	1	87
5	4.2	H_2O/EtOH (5:1 v/v)	Reflux	40 (min)	92
6	4.5	H_2O/EtOH (5:1 v/v)	Reflux	30 (min)	97
7	4.7	H_2O/EtOH (5:1 v/v)	Reflux	30 (min)	97
8	4.5	H_2O	Reflux	30 (min)	97
9	4.5	H_2O	RT	4	80
10	4.5	H_2O	80	1.5	90
11	4.5	H_2O	90	30 (min)	97
12[a]	0.05(g)	H_2O	90	5	25
13[b]	0.05 (g)	H_2O	90	2.5	45
14[c]	0.05 (g)	H_2O	90	2.5	45
15[d]	0.05 (g)	H_2O	90	2.5	70
16[e]	0.17 (g)	H_2O	90	2.5	55

Reaction conditions: benzaldehyde (0.5 mmol), barbituric acid (1 mmol), ammonium acetate (0.8 mmol) and solvent (5 mL).[a] The reaction was performed in the presence of Fe_3O_4 NPs.[b] The reaction was performed in the presence of Fe_3O_4@MCM-41 (**II**).[c] The reaction was performed in the presence of Fe_3O_4@ MCM-41-GPTMS (**III**).[d] The reaction was performed in the presence of Fe_3O_4@ MCM-41-GPTMS-Gu (**IV**).[e] The reaction was performed in the presence of Cu $(OAc)_2 \cdot H_2O$.

Table 3. One-pot synthesis of different structurally 5-phenyl-5,10-dihydropyrido[2,3-d:6,5-d′]dipyrimidine-2,4,6,8(1*H*,3*H*,7*H*,9*H*)-tetraone derivatives in the presence of Fe_3O_4@MCM-41-GPTMS-Gu-Cu^{II} under optimized condition.

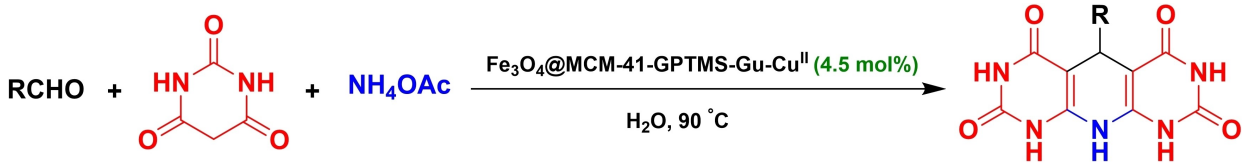

Entry	R	Product	Time (min)	Isolated Yield (%)
1	C_6H_5	**4a**	30	97
2	4-O_2N-C_6H_5	**4b**	25	97
3	4-NC-C_6H_5	**4c**	25	95
4	4-Cl-C_6H_5	**4d**	25	90
5	2-Cl-C_6H_5	**4e**	25	80
6	4-I-C_6H_5	**4f**	25	85
7	4-HO-C_6H_5	**4g**	35	90
8	2-HO-C_6H_5	**4h**	40	70
9	3,4-HO-C_6H_5	**4i**	35	85
10	4-H_3CO-C_6H_5	**4j**	30	75
11	4-H_3C-C_6H_5	**4k**	30	80
12	2-H_3C-C_6H_5	**4l**	35	75
13	4-$(H_3C)_2N$-C_6H_5	**4m**	30	70
14	1-H_7C_{10}	**4n**	30/10 h	65/65
15	2-H_7C_{10}	**4o**	40/10 h	65/65

further examined for the one-pot multicomponent reaction of aliphatic aldehydes with barbituric acid and ammonium acetate (Table 3, entries 14–15). Comparatively, aliphatic aldehydes resulted in the corresponding products with moderate yields and in longer reaction times. This catalytic system did not support the one-pot multicomponent reaction of heteroaromatic aldehydes (2-thiophene carbaldehyde, 4-pyridine carbaldehyde, and 2-furan carbaldehyde) with barbituric acid and ammonium acetate.

Most of the obtained 5-phenyl-5,10-dihydropyrido[2,3-d:6,5-d′]dipyrimidine-2,4,6,8(1*H*,3*H*,7*H*,9*H*)-tetraone derivatives (**4a**, **4b**, **4d**, **4e**, **and 4g–m**) were known, and their structures were confirmed by comparing their physical data (color and melting points) with those of authentic compounds which have been reported in the literature. The structure of the novel synthesized compounds (**4c**, **4f**, **4n**, **and 4o**) and some of the selected products were further recognized by FT-IR, ^{1}HNMR, and ^{13}CNMR spectroscopy and mass spectrometry as well. The elemental analysis technique was also employed for further characterization of the novel synthesized compounds. It is worth noting that the disappearance of the initial materials and the appearance of the product on TLC was used to monitor the reaction's progress and hence to confirm the completion of the reaction.

A recommended mechanism pathway for the synthesis of 5-phenyl-5,10-dihydropyrido[2,3-d:6,5-d′]dipyrimidine-2,4,6,8(1*H*,3*H*,7*H*,9*H*)-tetraone derivatives through the one-pot multicomponent reaction in the presence of Fe_3O_4@MCM-41-GPTMS-Gu-Cu^{II} is presented in Scheme 3, as reported previously.[22]

At first, the aldehyde carbonyl group becomes activated by donating a lone pair to Lewis acid sites (Cu^{II}) as well as the formation of a strong hydrogen bond between OH, NH, NH_2, and =NH of the anchored guanidine on magnetic mesoporous MCM-41 and a carbonyl group. Then, Knoevenagel dehydration condensation between the tautomeric form of barbituric acid **I** and activated aldehyde resulted in the generation of benzylidine barbiturate **II**. Subsequently, Michael's addition between intermediate **II** and the second molecule of barbituric acid **I** led to the formation of the adduct **III**. In the next step, the nucleophilic attack of ammonium acetate to the adduct **III** afforded the intermediate **IV**, which subsequently tautomerizes to intermediates **V** and **VI**, respectively. Eventually, Michael adduct **VI** (the more stable tautomeric form) takes part in a facile intramolecular ring-closure *via* a 6-exo-trig process to generate the desired product **VII** on removing water as green waste (Scheme 4). Finally, Fe_3O_4@MCM-41-GPTMS-Gu-Cu^{II} re-introduced to another catalytic cycle.

It is worth noting that the recycling and recovery of the heterogeneous catalytic systems are one of the main advantages of the economic, industrial, and environmental perspectives. In this regard, the recyclability potential of the prepared catalyst was checked for the model reaction under the standard conditions. For this purpose, after the completion of the reaction, the Fe_3O_4@MCM-41-GPTMS-Gu-Cu^{II} nanocatalyst was separated from the reaction media, and recovered using a permanent magnet and washed with deionized water (3× 5 mL), ethanol (3×5 mL) to remove excess reagents and organic residues. Afterward, it was dried under a vacuum at 60 °C and consequently used for the subsequent experiments. It became apparent that the nanocatalyst can be reused successfully with satisfactory yields compared to the fresh catalyst without any deactivation even after 5 runs (Figure 13).

Interestingly, a comparison of the FT-IR spectrum of the fresh and the 5th reused nanocatalyst showed the remaining

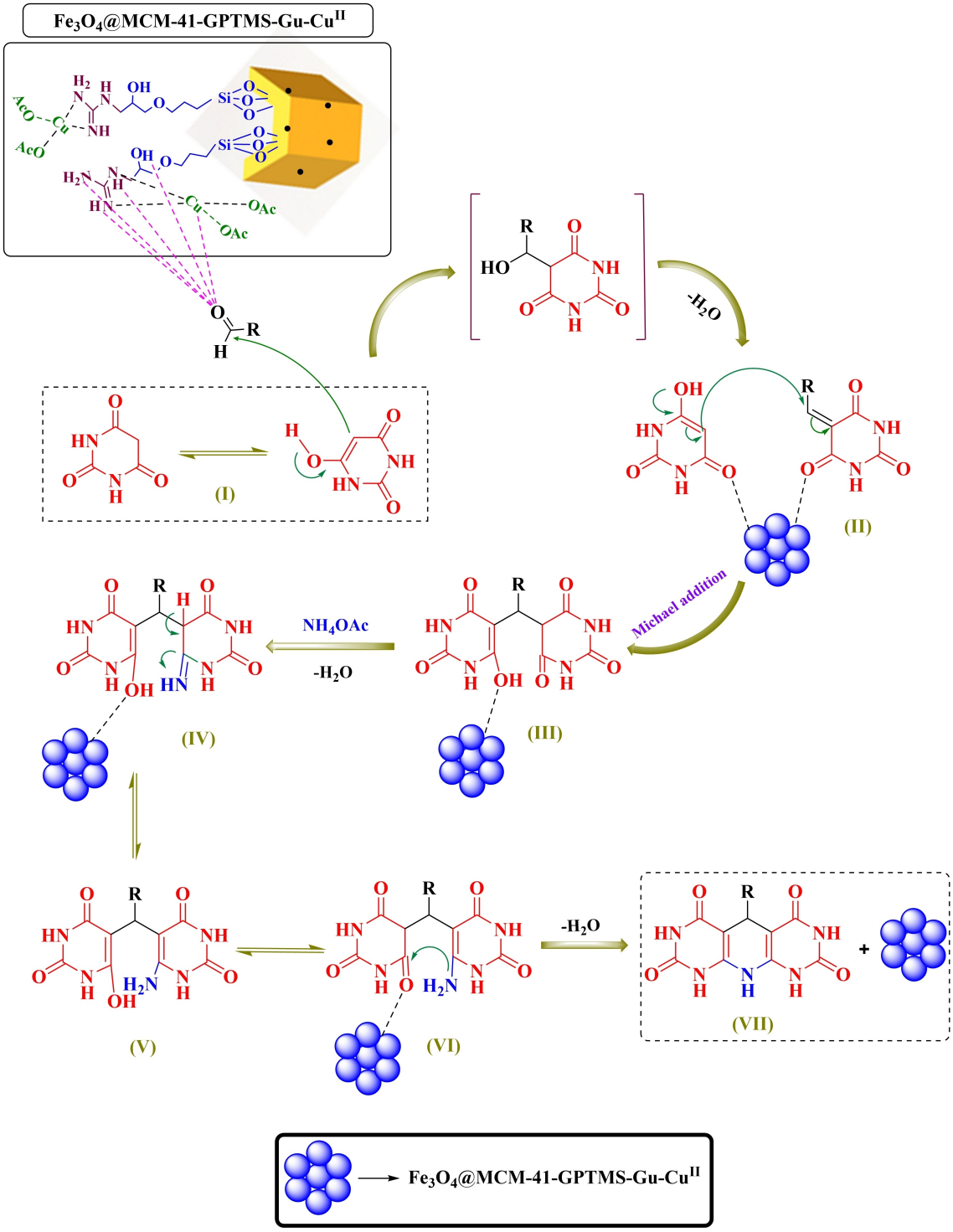

Scheme 4. Recommended mechanism pathway for the synthesis of 5-phenyl-5,10-dihydropyrido[2,3-d:6,5-d']dipyrimidine-2,4,6,8(1*H*,3*H*,7*H*,9*H*)-tetraone derivatives catalyzed by Fe_3O_4@MCM-41-GPTMS-Gu-Cu^{II} (**V**).

three absorption bands at around 2924–2826 cm^{-1}, 1644 cm^{-1} and 1063

cm^{-1}, which were due to the stretching vibration of CH_2 groups, stretching vibration of ν C=N, and stretching vibration of Si–O–Si of the MCM-41, establishing the stability of the structure of nanocatalyst after five cycles (compare Figure 1e and f). Likewise, the obtained XRD results exhibited that the chemical structure of nanocatalyst has no significant difference even after five runs (compare Figure 2b and c, and Figure 3b and c). Also, the obtained SEM images of the reused nanocatalyst as compared to fresh nanocatalyst established that the nanocatalyst has an approximately spherical shape, confirming

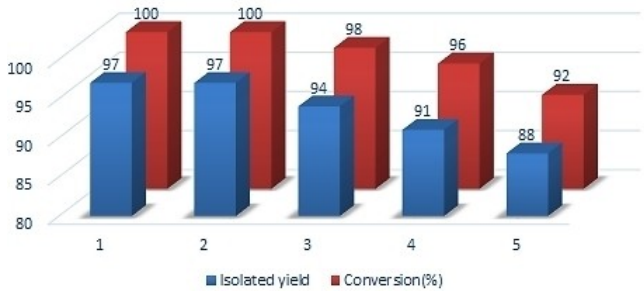

Figure 13. Synthesis of 5-phenyl-5,10-dihydropyrido[2,3-d:6,5-d′]dipyrimidine-2,4,6,8(1*H*,3*H*,7*H*,9*H*)-tetraone (**4a**) in the presence of reused Fe_3O_4@MCM-41-GPTMS-Gu-Cu^{II} (**V**).

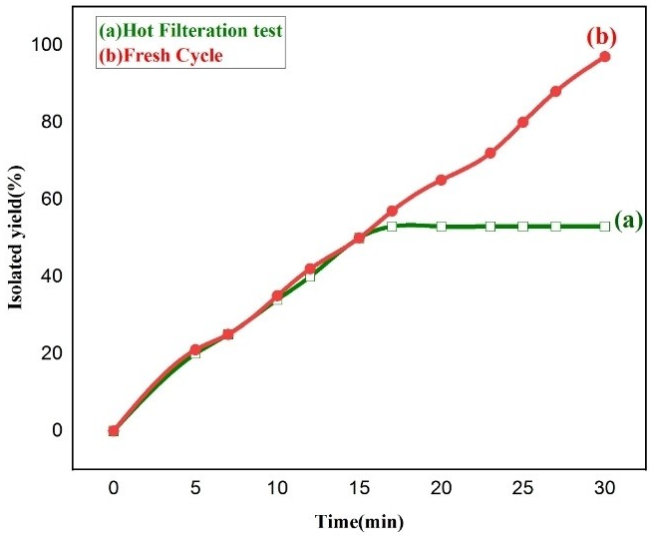

Figure 14. Time-dependent correlation of the product yield in hot filtration test.

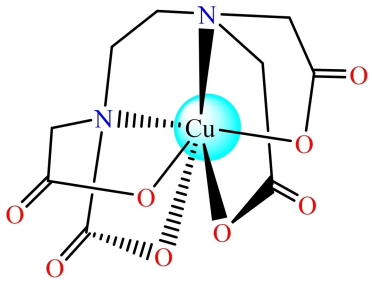

Scheme 5. The chemical structure of the Cu^{II} (EDTA) complex.

the stable morphology of nanocatalyst even after being used several times (compare Figure 5b and c). Besides, the XPS study of the fifth recovered nanostructured catalyst showed that all Cu species are in a +2 oxidation state (Figure 12b). Similarly, the ICP analysis demonstrated that the freshly prepared catalyst contains 57.150 ppm/or 0.057 g/or 0.900 mmol of Cu per 1 g of catalyst, while this amount decreased to 56.642 ppm/or 0.056 g/or 0.892 mmol of Cu per 1 gr of 5th reused. This indicates that 8% of Cu^{II} leached from the structure of the catalyst after five runs.

Hot filtration test

To check the heterogeneous nature of the nanocatalyst, a hot filtration test was performed. At first, the model reaction was conducted under the optimized reaction condition for15 minutes, and then the catalyst was magnetically separated from the reaction medium while the reaction proceeded approximately 50%. Then, the reaction was continued and monitored (by TLC) for another 15 minutes under the same reaction conditions without any catalyst. It appeared that the reaction did not proceed further after the removal of the nanocatalyst (Figure 14). This result proposed that no leaching of Cu^{II} took place in the reaction mixture, and thus, the nanocatalyst has a truly heterogeneous nature, and stable during the catalytic reaction.

Poisoning test

To further discern the true nature (homogeneous or heterogeneous) of the nanocatalyst, a poisoning test was done under the optimized reaction conditions in two separate flasks in the presence and in the absence of ethylenediaminetetraacetic acid (EDTA), as an excellent scavenger to grab homogeneous Cu^{II} species because of its high affinity to the formation of a stable complex with the soluble Cu^{II} ions (Scheme 5).[49] Toward this point, the reaction progress was monitored by TLC. The obtained results of Figure 15 displayed that the yield of the reaction experienced no noticeable decrease, confirming the fact that no leaching of Cu^{II} ions took place in solution during the reaction and can prove the specific heterogeneous nature of the nanocatalyst.

To show the merits of the proposed catalytic system, the efficiency of the present nanocatalyst was compared with those obtained using other catalysts that were applied in the one-pot preparation of 5-phenyl-5,10-dihydropyrido[2,3-d:6,5-d′]dipyrimidine-2,4,6,8(1*H*,3*H*,7*H*,9*H*)-tetraone (4a) (Table 4).

Although, each of these catalytic systems has their superiority, as can be apparently seen from Table 4, prolonged reaction time to obtain the appropriate product (Table 4, entry 1 and 4), the use of a toxic solvent (Table 4, entry 2 and 5), tedious reaction procedure (unfeasible for reaction monitoring (Mw), difficult to control the temperature (US), unsuitable for scale-up) (Table 4, entries 3 and 4), and homogenous catalytic system (difficult separation from products) (Table 4, entry 5), are the drawbacks of some of these methods. Therefore, Fe_3O_4@MCM-41-GPTMS-Gu-Cu^{II} as a heterogeneous and green nanocatalyst is more effective than most of the catalysts concerning the reaction time, green condition reaction, high yield of the products, and especially easy recovering potential of the catalyst from the reaction mixture. The superiority of the

Table 4. Comparison between the catalytic efficiency of Fe_3O_4@MCM-41-GPTMS-Gu-Cu^{II} (**V**) and some other catalysts for the synthesis of 5-phenyl-5,10-dihydropyrido[2,3-d:6,5-d′]dipyrimidine-2,4,6,8(1*H*,3*H*,7*H*,9*H*)-tetraone (4a).

Entry	Catalyst	Solvent	Temp.(°C)	Time(h)	Yield (%)	Ref.
1	Catalyst-free	Water/ethanol(5:1 v/v)	100	10	85	[50]
2	Fe_3O_4/SiO_2-*N*-propyl-benzoguanamine-SO_3H	Ethanol (5 mL)	50	10 (min)	94	[22]
3	β-cyclodextrin	Ethanol (5 mL)	60/US	1	90	[51]
4	Catalyst-free	Water	MW	2	82	[52]
5	DIPEA [a]	Acetonitrile	RT	45 (min)	95	[33]
6	Fe_3O_4@MCM-41/GPTMS-Gu-Cu^{II}	Water	90	30 (min)	97	Present study

[a] Diisopropylethylammonium acetate (DIPEA).

current approach over the previously reported methods was well-established thanks to the results obtained.

Conclusion

In summary, in order to make an excellent contribution to the development of green chemistry, Fe_3O_4@MCM-41-GPTMS-Gu-Cu^{II} was successfully fabricated as a new magnetic nanocatalyst and characterized using several techniques (FT-IR, XRD, small-angle XRD, BET, SEM, EDX, EDX-mapping, TEM, TGA, VSM, XPS, and ICP). The catalytic performance of Fe_3O_4@MCM-41-GPTMS-Gu-Cu^{II} with narrow particle size distribution (8–25 nm) and super magnetic behavior was investigated in a one-pot multi-component reaction towards the formation of 5-phenyl-5,10-dihydropyrido[2,3-d:6,5-d′]dipyrimidine-2,4,6,8(1*H*,3*H*,7*H*,9*H*)-tetraone derivatives in a green media. This magnetic nanocatlyst has heterogeneous nature and shows high durability according to the hot-filtration test, controlled poisoning experiment studies, and spectroscopic and microscopic results of the 5th reused catalyst. Efficiency, environmental tolerability, excellent yield of products, short reaction times, excellent functional group compatibility, clean reaction profile, easy experimental and work-up procedures, and using H_2O as the reaction media are consistent advantages of the present methodology.

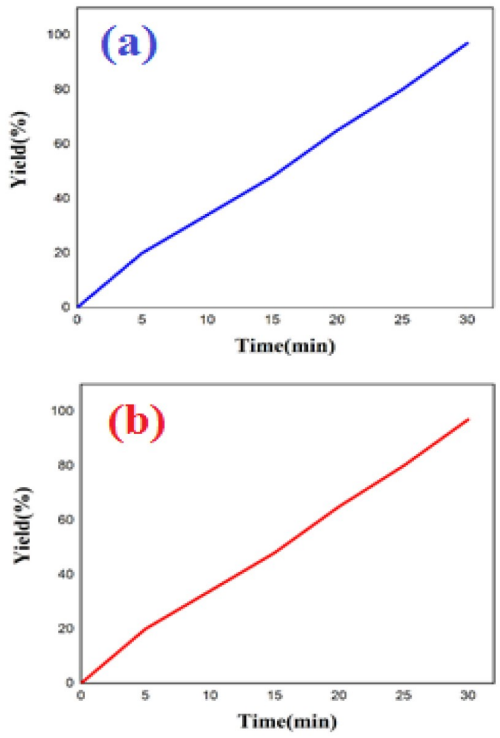

Figure 15. Time-dependent correlation of the product yield of the model reaction in the presence (a) and in the absence (b) of EDTA (ethylenediaminetetraacetic acid).

Supporting Information Summary

Experimental section, FT-IR, ^{1}HNMR, ^{13}CNMR, and Mass spectrum analysis of products were described.

Acknowledgements

The authors gratefully acknowledge the partial support of this study by Ferdowsi University of Mashhad Research Council (Grant No. p/3/49110).

Conflict of Interest

The authors declare no conflict of interest.

Keywords: Fe_3O_4@MCM-41-GPTMS-Gu-Cu^{II} · magnetic mesoporous MCM-41 · one-pot multicomponent synthesis · dihydropyrido[2,3-d:6,5-d′]dipyrimidines

[1] T. Deligeorgiev, N. Gadjev, A. Vasilev, S. Kaloyanova, J. J. Vaquero, J. Alvarez-Builla, *Mini-Rev. Org. Chem.* **2010**, *7*, 44–53.
[2] M. R. Mousavi, M. T. Maghsoodlou, *J. Iran. Chem. Soc.* **2015**, *12*, 743–749.
[3] J. C. Védrine, *Catalysts* **2017**, *7*, 341.
[4] M. E. Ali, M. M. Rahman, S. M. Sarkar, S. B. A. Hamid, *J. Nanomater.* **2014**, *2014*, 1–23.
[5] A. Moaddeli, M. Abdollahi-Alibeik, *J. Porous Mater.* **2017**, *25*, 147–159.
[6] K. Alizadeh, E. Khaledyan, Y. Mansourpanah, *J. Water Environ. Nanotechnol.* **2018**, *3*, 243–253.
[7] D. da Costa Cabrera, E. Santa-Helena, H. Leal, R. de Moura, L. Nery, C. Gonçalves, D. Russowsky, M. Montes D'Oca, *Bioorg. Chem.* **2019**, *84*, 1–16.
[8] S. Bhaskaruni, S. Maddila, W. van Zyl, S. Jonnalagadda, *Catal. Today.* **2018**, *309*, 276–281.
[9] A. Khazaei, A. R. Moosavi-Zare, H. Afshar-Hezarkhani, V. Khakyzadeh, *Eurasian Chem. Commun.* **2020**, *2*, 27–34.
[10] G. M. Reddy, J. Raul Garcia, N. B. Reddy, G. V. Zyryanov, G. Yuvaraja, *J. Heterocycl. Chem.* **2019**, *56*, 845–849.

[11] A. M. Vijesh, A. M. Isloor, S. K. Peethambar, K. N. Shivananda, T. Arulmoli, N. A. Isloor, *Eur. J. Med. Chem.* **2011**, *46*, 5591–5597.
[12] M. G. Sharma, R. M. Vala, H. M. Patel , *RSC Adv.* **2020**, *10*, 35499–35504.
[13] L. L. Acković, I. Zeković, T. Dramićanin, R. Bro, M. D. Dramićanin, *Polycyclic Aromat. Compd.* **2019**, *39*, 395–485.
[14] R. M. Vala, D. M. Patel, M. G. Sharma, H. M. Patel, *RSC Adv.* **2019**, *9*, 28886–28893.
[15] M. G. Sharma, R. M. Vala, D. M. Patel, I. Lagunes, M. X. Fernandes, J. M. Padrón, V. Ramkumar, R. L. Gardas, H. M. Patel , *ChemistrySelect.* **2018**, *3*, 12163–12168.
[16] H. M. Patel, D. P. Rajani, M. G. Sharma, H. G. Bhatt, *Lett. Drug Des. Discovery* **2019**, *16*, 119–126.
[17] W. Huang, J. Xu, C. Liu, Z. Chen, Y. Gu, *J. Org. Chem.* **2019**, *84*, 2941–2950.
[18] H. M. Patel, *Curr. Bioact. Compd.* **2018**, *14*, 278–288.
[19] D. M. Patel, H. M. Patel, *ACS Sustain. Chem. Eng.* **2019**, *7*, 18667–18676.
[20] D. M. Patel, R. M. Vala, M. G. Sharma, D. P. Rajani, H. M. Patel, *ChemistrySelect.* **2019**, *4*, 1031–1041.
[21] D. M. Patel, M. G. Sharma, R. M. Vala, I. Lagunes, A. Puert, J. M. Padrón, D. P. Padrón, D. P. Rajani, H. M. Patel, *Bioorg. Chem.* **2019**, *86*, 137–150.
[22] M. Gholami Dehbalaei, N. Foroughifar, A. Khajeh-Amiri, H. Pasdar, *J. Chin. Chem. Soc.* **2018**, *65*, 1356–1369.
[23] N. Tripathi, Advances in Water Pollution Monitoring and Control. **2020**, 79–84.
[24] D. Ashokkumar, G. Ramalingam, M. Gopalakrishnan, *Asian J. Chem.* **2019**, *31*, 2976–2980.
[25] G. Brahmachari, K. Nurjamal, I. Karmakar, S. Begam, N. Nayek, B. Mandal, *ACS Sustainable Chem. Eng.* **2017**, *5*, 9494–9505.
[26] C. Verma, M. A. Quraishi, K. Kluza, M. Makowska-Janusik, L. O. Olasunkanmi, E. E. Ebenso, *Sci. Rep.* **2017**, *7*, 44432.
[27] H. Naeimi, A. Didar, Z. Rashid, Z. Zahraie, *J. Antibiot.* **2017**, *70*, 845–852.
[28] K. T. Patil, P. P. Warekar, P. T. Patil, S. S. Undare, G. B. Kolekar, P. V. Anbhule, *J. Heterocycl. Chem.* **2017**, 11–16.
[29] M. N. Nasr, M. M. Gineinah, *Arch. Pharm. Pharm. Med. Chem.* **2002**, *6*, 289–295.
[30] Z. Toobaei, R. Yousefi, F. Panahi, S. Shahidpour, M. Nourisefat, M. M. Doroodmand, A. Khalafi-Nezhad, *Carbohydr. Res.* **2015**, *411*,22–32.
[31] P. M. Petersen, W. Wu, E. E. Fenlon, S. Kim, S. C. Zimmerman, *Bioorg. Med. Chem.* **1996**, *4*, 1107–1112.
[32] A. Kohzadian, A. Zare, *Silicon.* **2020**, *12*, 1407–1415.
[33] M. R. Bhosle, L. D. Khillare, J. R. Mali, A. P. Sarkate, D. K. Lokwani, S. V. Tiwari, *New J. Chem.* **2018**, *42*, 18621–18632.
[34] H. Naeimi, A. Didar, Z. Rashid, Z. Zahraie, *J. Antibiot. Res.* **2017**, *70*, 845–852.
[35] a) Z. Zarei, B. Akhlaghinia, *Turk. J. Chem.* **2018**, *42*, 170–191; b) Z. Zarei, B. Akhlaghinia, *New J. Chem.* **2017**, *41*, 15485–15500; c) A. Mohammadinezhad, B. Akhlaghinia, *Catal. Lett.* **2020**, *150*, 332–352; d) M. A. Erfan, B. Akhlaghinia, S. S. E. Ghodsinia, *ChemistrySelect.* **2020**, *5*, 2306–2316; e) B. Akhlaghinia, P. Sanati, A. Mohammadinezhad, Z. Zarei, *Res. Chem. Intermed.* **2019**, *45*, 3215–3235; f) Z. Zarei, B. Akhlaghinia, *RSC Adv.* **2016**, *6*, 106473–106484; g) N. Mohammadian, B. Akhlaghinia, *Res. Chem. Intermed.* **2019**, *45*, 4737–4756; h) R. Jahanshahi, B. Akhlaghinia, *Catal. Lett.* **2017**, *147*, 2640–2655.
[36] B. Liu, M. Liu, L. Liang, J. Sun, *Catalysts* **2015**, *5*, 119–130.
[37] F. Noruzian, A. Olyaei, R. Hajinasiri, M. Sadeghpour, *Synth. Commun.* **2019**, *49*, 2717–2724.
[38] a) J. Safaei-Ghomi, H. Shahbazi-Alavi, P. Babaei, *Z. Naturforsch. B.* **2016**, *71*, 1–8; b) S. Villa, P. Riani, F. Locardi, F. Canepa, *Materials* **2016**, *9*, 826.
[39] M. Behbahani, A. A. Akbari, M. M. Amini, A. Bagheri, *Anal. Methods* **2014**, *6*, 8785–8792.
[40] F. Guodong, G. Mingming, L. Qi, M. Hongyu, L. Guanghua, M. Qiang, F. Qiang, H. Yanfu, S. Zhiguang, *New J. Chem.* **2016**, *40*, 8444–8450.
[41] Y. Shao, T. Jing, J. Tian, Y. Zheng, *RSC Adv.* **2015**, *5*, 103943–103955.
[42] M. Mazhar, S. M. Hussain, F. Rabbani, G. Kociok-Köhn, K. C. Molloy, *Bull. Korean Chem. Soc.* **2006**, *27*, 1572–1576.
[43] A. Ahmad, M. H. Razali, K. Kassim, K. A. M. Amin, *J. Porous Mater.* **2018**, *25*, 433–441.
[44] N. Akbarikalani, K. Amiri, A. Al-Harrasi, S. Balalaie, *RSC Adv.* **2020**, *10*, 10577–10583.
[45] a) N. H. Z. Abidin, W. N. W. Ibrahim, N. S. M. Hanapi, N. Saim , *Indones. J. Chem.* **2020**, *20*, 729–745; b) S. Popescu, I. L. Ardelean, D. Gudovan, M. Rădulescu, D. Ficai, A. Ficai, B. Ş. Vasile, E. Andronescu, *Rom. J. Morphol. Embryol.* **2016**, *57*, 483–489; c) W. Xie, X. Zang, *Food Chem.* **2016**, *194*, 1283–1292.
[46] E. Tezel, H. E. Figen, S. Z. Baykara, *Int. J. Hydrogen Energy* **2019**, *44*, 9930–9940.
[47] A. Ulu, S. A. A. Noma, S. Koytepe, B. Ates, *Appl. Biochem. Biotechnol.* **2019**, *187*, 938–956.
[48] Y. Wang, J. Liu, Ch. Xia, *Adv. Synth. Catal.* **2011**, *353*, 1534–1542.
[49] E. R. Taqanaki, R. Heidari, M. Monfared, L. Tayebi, A. Azadi, F. Farjadian, *Int. J. Nanomed.* **2019**, *14*, 7781–7792.
[50] N. Azizi, A. Mobinikhaledi, A. K. Amiri, H. Ghafuri, *Res. Chem. Intermed.* **2012**, *38*, 2271–2275.
[51] C. Jadhav, L. D. Khillare, M. R. Bhosle, *Synth. Commun.* **2018**, *48*, 233–246.
[52] M. Kidwai, K. Singhal, *Can. J. Chem.* **2007**, *85*, 400–405.

Submitted: October 27, 2020
Accepted: December 16, 2020